





PAPER

[View Article Online](#)
[View Journal](#) | [View Issue](#)


Cite this: *Green Chem.*, 2022, **24**, 5291

Biobased thin-film composite membranes comprising priamine–genipin selective layer on nanofibrous biodegradable polylactic acid support for oil and solvent-resistant nanofiltration†

Cong Yang, ^a Fuat Topuz, ^a Sang-Hee Park ^{a,b} and Gyorgy Szekely ^{*a}

Green thin-film composite (TFC) membranes can offer a sustainable solution for the separation of complex mixtures in aqueous and organic solvent nanofiltration (OSN). However, the fabrication of TFC membranes has relied on toxic petrochemical-based monomers, solvents, and supports. Herein, we developed a green TFC membrane using solely sustainable resources. A fully biodegradable electrospun nanofibrous support comprising polylactic acid (PLA) and gelatin (as the interlayer) was developed for the TFC membranes. Dimethyl carbonate and water, as green solvents, were used for the dissolution of PLA and gelatin, respectively. The incorporation of the gelatin interlayer enhanced the hydrophilicity of the support, leading to the homogeneous adhesion of the TFC membrane. Green polyamide TFC membranes were fabricated on the porous support via the interfacial polymerization of natural monomers, namely the plant-based genipin in the aqueous phase, and priamine in the green organic solvent eucalyptol. The biodegradability of the support was demonstrated using proteinase K within 10 h. The green TFC membrane showed outstanding acetone permeance up to $10 \text{ L m}^{-2} \text{ h}^{-1} \text{ bar}^{-1}$ with a molecular weight cut-off in the range of 178–391 g mol^{-1} . The optimized membrane demonstrated an oil removal rate of 99.6% in the produced water treatment at a water permeance of $5.6 \text{ L m}^{-2} \text{ h}^{-1} \text{ bar}^{-1}$. The robustness of the TFC membrane was evidenced through continuous crossflow filtration under 30 bar over seven days. The sustainability of the membrane was assessed and compared against green and conventional membranes. Overall, the excellent solvent stability and OSN performance of the ecofriendly TFC membranes can lead to new advances in sustainable membrane manufacturing.

Received 18th April 2022,
Accepted 14th June 2022

DOI: 10.1039/d2gc01476a

rsc.li/greenchem

Introduction

Reducing costs while enhancing sustainability through molecular-level separation is becoming essential in industry. Compared to conventional energy-demanding technologies, advanced membrane separation techniques, such as organic solvent nanofiltration (OSN), show many advantageous properties, including compact modules, mild operational conditions, and a low carbon footprint.¹ Currently, thin-film composite (TFC) membranes and polymeric integrally skinned asymmetric (ISA) membranes are massively used in OSN,² while the former shows significant advantages over the latter.

For example, as the composite layers can be modified independently (Fig. 1), TFC membranes can be designed more flexibly to alter molecular-level membrane properties by utilizing organic chemistry.³

However, TFC membranes are often synthesized using petroleum-based raw materials. Thus, recent studies have been devoted to investigating sustainable and green TFC fabrication systems.^{4,5} Green solvents, including decanoic acid,⁶ *p*-cymene,⁷ eucalyptol,⁸ TamiSolve NxG,⁹ and α -pinene,^{10,11} were adopted for the fabrication of TFC membranes using interfacial polymerization (IP). In addition, ionic liquids have been proposed for fabricating the TFC membranes for OSN.¹² A low-temperature condensation process was also developed for the fabrication of polyimide TFC membranes on nanofibrous poly(amic acid) supports.¹³ Catechin¹¹ and quercetin¹⁰ have been proposed as green monomers for IP to form selective layers on cellulose supports. However, in both cases, fossil-based toxic terephthaloyl chloride was used as the comonomer, and *N,N*-dimethylformamide (DMF) was used to dissolve cellulose for the preparation of the support layer.

^aAdvanced Membranes and Porous Materials Center, Physical Science and Engineering Division (PSE), King Abdullah University of Science and Technology (KAUST), Thuwal, 23955-6900, Saudi Arabia. E-mail: gyorgy.szekely@kaust.edu.sa, www.szekelygroup.com

^bDepartment of Chemical Engineering, Changwon National University (CNU), Changwon 51140, Korea

† Electronic supplementary information (ESI) available. See DOI: <https://doi.org/10.1039/d2gc01476a>



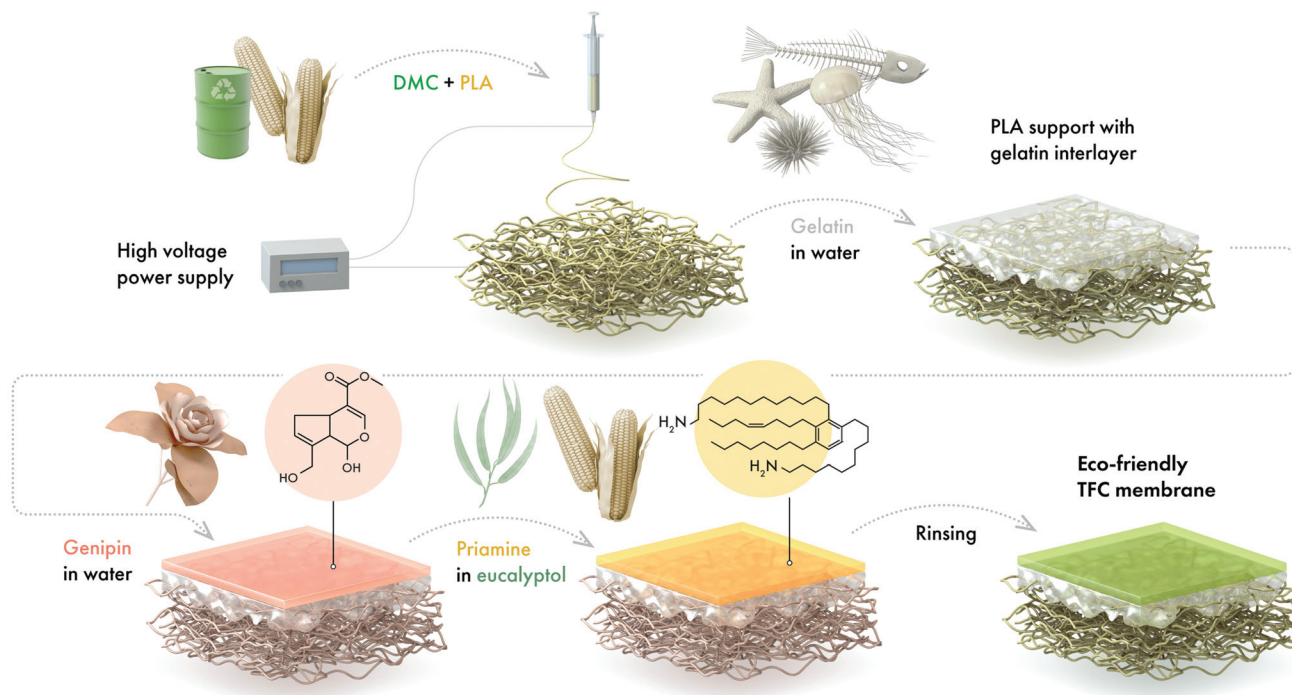


Fig. 1 Schematic fabrication process of the green thin-film composite (TFC) membrane using solely sustainable resources. A fully biodegradable electrospun polylactic acid (PLA) mat was developed as a highly porous membrane support with a gelatin interlayer. Green solvents were used in all the fabrication steps. The interfacial polymerization (IP) reaction utilized plant-based materials (genipin and priamine).

Recently, plant-derived monomers, including priamine and tannic acid, were used for IP, and recycled PET was used as the support.⁷ Another green TFC fabrication system was composed of chitosan derived from shrimp shells and biomass-based building block 2,5-furandicarboxaldehyde based on a recycled PET support.⁸ The pore size of the selective layer was controlled using green solvent Tamisolve.

Electrospinning is a scalable technique that can be used at room temperature under ambient pressure.¹⁴ Electrospun nanofibers offer flexibility, stretchability, and large porosity, which benefit solvent transport and robustness, leading to a highly permeable TFC membrane.¹⁵ The coupling of electrospun nanofibers with TFCs enhanced the polar solvent separation.¹⁶ An electrospun mat-supported TFC was also demonstrated for OSN.^{13,17–21}

However, traditional polyacrylonitrile polymer and harsh and toxic solvents, including DMF, *N*-methyl-2-pyrrolidinone (NMP), and cyclohexane, are commonly used during the fabrication of TFC membranes and their supports. As this deviates from the basic 12 principles of green chemistry, greener and more environmentally benign systems must be developed. Polylactic acid (PLA) is a natural polymer that can be biodegraded by attacking the ester groups in the polymer chain.²² It is used as a support material due to its renewability and biodegradability^{23,24} and can be electrospun to obtain nanofibers.²⁵ Studies have been conducted on the PLA solution preparation using traditional solvents (*e.g.*, chloroform and DMF).^{26–28} Dimethyl carbonate (DMC) is an environmentally

friendly solvent that can improve the renewability of polysaccharides, sugar-derived platform molecules, lignin-based phenolic compounds, glycerol, and fatty acids;^{4,29} therefore, DMC can dissolve PLA.^{30,31}

Due to the chemical nature of PLA, electrospun nanofibrous supports are hydrophobic with a water contact angle in the range of 128°–136°. This hinders the formation of the polyamide layer in a TFC membrane as the support should be hydrophilic enough to uptake monomers from the aqueous phase.³² In addition, the loosened stacked fibers may lead to defects in the final TFC membranes. To tackle this problem, an interlayer is added when using electrospun nanofibers as TFC supports.^{33–35} However, most of the demonstrated applications were based on forward osmosis rather than OSN. Moreover, gelatin is utilized as a natural and green material, which provides sufficient interfacial coverage. Hence, a gelatin interlayer can be coupled with TFC fabrication to improve the mechanical properties of the composite membrane.

Genipin is a colorless cyclopentapyrane-type monoterpenoid (iridoid) produced from the hydrolysis of geniposide extracted from the fruits of *Gardenia* (*Gardenia Jasminoides* J. Ellis).³⁶ Owing to its relatively low toxicity, genipin has been extensively used as a covalent cross-linker for polysaccharides and proteins in foodstuff packaging^{37,38} or tissue engineering.³⁹

Annually, polymeric membrane fabrication produces 50 billion liters of wastewater contaminated by toxic solvents, including DMF and NMP.⁴⁰ To reduce environmental pol-



lution, green solvents are now being considered as an alternative to hazardous solvents used in traditional chemical production.⁴¹ Eucalyptol is a bicyclic ether originally derived from eucalyptus tree leaves. Previously, a naturally derived monomer, priamine, was dissolved in eucalyptol as an organic phase for TFC fabrication. The synthesized membrane had the lowest hazardous level without compromising the OSN performance.⁷

Herein, we present a solely green TFC fabrication system that contains biodegradable green electrospun support, green solvents, green monomers, and a scalable electrospinning technique. In line with the 5th and 7th principles of green chemistry and the 12th sustainable development goal of the United Nations, the use of green solvents and renewable feedstocks is essential for long-term sustainable development. The membranes demonstrated strong mechanical and chemical stability and excellent performance in OSN and oil-in-water separation.

Results and discussion

Green TFC support *via* electrospinning

To optimize the fiber formation conditions, polymer concentrations (5–15 w/v%, refer to section S1 in the ESI†) and salt concentrations (1–15 w/w%, refer to section S1 in the ESI†) were investigated, followed by the adjustment of operational parameters, including applied voltage (10–20 kV, refer to section S1 in the ESI†), polymer solution flow rate (0.25–2 mL h⁻¹, refer to section S1 in the ESI†), and TCD (50–200 mm, refer to section S1 in the ESI†).

Fig. 2 reveals the properties of the green electrospun PLA support. The detailed electrospun PLA fiber size fine-tuning process is shown in the ESI†, the SEM images of the uniform electrospun fibers are shown in Fig. 2a, the corresponding fiber size distribution is shown in Fig. 2b, and the cross section is shown in Fig. 2c. A clear transforming trend from the beaded fiber to the bead-free fiber was observed when increasing the PLA concentration, refer to section S1 in the ESI†, along with the porous structure. The bead formation could be attributed to the elasticity of the solution. In particular, solutions with low extensional viscosity and low relaxation time are prone to form beads.⁴² The mechanism could be explained by the suppression of Rayleigh instability driven by surface tension by the viscoelastic behavior of the fluid jet. Increasing the PLA content boosted the viscoelasticity, and eventually eliminated beads formation.⁴³ The addition of TBAB facilitated the formation of uniform and thinner nanofibers, and the average fiber diameter decreased from 939 nm at 2.5 w/w% TBAB to 282 nm at 15 w/w% TBAB with a PLA concentration of 12.5 w/v% (refer to section S1 in the ESI†). The nanofibers produced under 10 kV had a mean diameter of 410 nm, which decreased to 377 nm when the voltage increased to 20 kV. Most uniform nanofibers were prepared under an applied voltage of 15 kV (refer to section S1 in the ESI†). Similar to previous reports,⁴⁴ the increase in flow rate resulted in thicker fibers, and eventually, beaded fibers were observed. This can be attributed to the high volume and initial diameter of the electrospinning jet, resulting in bending instability and, in turn, increasing the fiber diameter. Figure in section S1 in the ESI† shows the increase in the

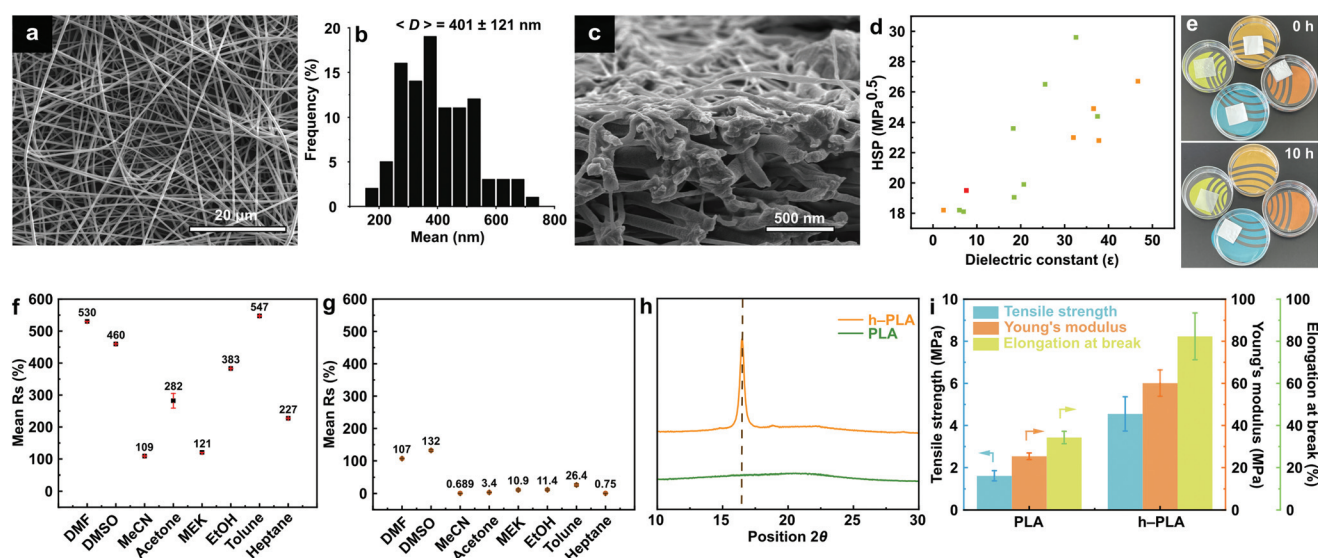


Fig. 2 h-PLA support characterization: the scanning electron microscope (SEM) image of the mat surface (a), the fiber size distribution (b), and the cross section (c), PLA support solubility as a function of the Hildebrand solubility parameter *versus* the dielectric constant of organic solvents (d), where the green dots refer to the soluble PLA support, while the red dots refer to the insoluble PLA mat, and the orange dots represent the swollen PLA support in the given solvents, the biodegradation results of the h-PLA mats with proteinase K (e), the swelling tests of the h-PLA support in organic solvents (f) and after the incorporation of the free-standing selective layer (g), the X-ray diffraction (XRD) patterns of the optimized PLA mat before and after hot annealing (h), and the dynamic mechanical analysis (DMA) results of the optimized PLA mat and the h-PLA mat (i).



mean diameter of the fibers from 309 to 987 nm as the flow rate increased from 0.25 to 1 mL h⁻¹, while the applied voltage was kept constant at 15 kV. At the optimum flow rate, the distribution of the fiber diameters is the narrowest. Finally, the effect of the TCD was also studied by altering the value from 50 to 200 mm, as shown in section S1 in the ESI† and the optimum TCD was found to be 100 mm with uniform fiber formation. The support produced using 12.5 w/v% PLA, 10 w/w% TBAB, an applied voltage of 15 kV, a flow rate of 0.5 mL h⁻¹, and a TCD of 100 mm was used to fabricate TFC membranes. The optimized PLA support exhibited a mean diameter of 401 nm, a wide open surface, and interconnected pores, which provided an effective dispersion of monomers, making it a promising green support material for TFC fabrication. The electrospinning of PLA from DMC solutions produced ultrafine nanofibers in the presence of the ammonium salt additive. Besides its green nature, the use of DMC led to a porous fiber structure because of its low boiling point of 90 °C. The use of salt additive improved the electrospinnability of PLA solutions, and allowed tailoring of the pore structure of the resultant fibers. Furthermore, unlike PLA fibers electrospun from dichloromethane, chloroform and trifluoroethanol, electrospinning from DMC solutions in the presence of TBAB resulted in very thin and more uniform fiber morphology.⁴⁵ The optimized h-PLA support was found to be stable under ketones and alcohols (Fig. 2d and section S2 in the ESI†), indicating that the electrospun nanofibrous support can be applied to the aforementioned organic solvent systems during TFC fabrication.

The biodegradability of the nanofibrous PLA membrane support was tested using proteinase K (refer to section S5 in the ESI†).⁴⁶ Unlike the PP membrane support in the green dish, the PLA membrane supports in orange and red dishes started to degrade upon 2 h of contact time with the enzymatic solution, and the biodegradation was completed after 10 h of enzymatic digestion, as shown in Fig. 2e. The successful biodegradation of the membrane support aids to close the sustainability loop of membrane materials. Our approach aims to address some of the 12 principles of green chemistry and engineering as well as the United Nations' Sustainable Development Goals by minimizing waste and designing for degradation.

The swelling ratios of the optimized electrospun h-PLA support and the free-standing selective layer in various organic solvents are shown in Fig. 2f and g, respectively.

The detailed data can be found in section S3 in the ESI†. The h-PLA support uptakes more solvent (swelling ratio ranging from 109% to 547%) compared to the free-standing selective layer from (0.75 to 1.32%). Despite their swelling, the prepared TFC membrane and its support can withstand common solvents. The difference in the swelling ratios of the membrane and the support may cause the detachment of the selective layer from the support. Nonetheless, in this study, this was not observed for any of the solvents and during the long-term filtration tests, verifying the excellent adhesion between the individual components of the PLA support-gelatin interlayer-polyamide membrane system.

The wide-angle XRD patterns are shown in Fig. 2h, and a clear peak at 16.8° was found in the spectrum of h-PLA, indicating that the hot annealing process below the melting point of the polymer helped with the atomic-level polymer chain self-assembly and enhanced the extensive crystallization of the polymer chains.⁴⁷ Therefore, the mechanical properties of the electrospun nanofibers improved after the hot annealing process, which was also supported by the DMA results (Fig. 2i, section S4 in the ESI†). We observed an increase in tensile strength from 1.62 to 4.55 MPa, and Young's modulus from 25.36 to 60.12 MPa because of the hot annealing process, indicating better mechanical properties of the optimized PLA support. This observation is in line with the literature on electrospun fibrous mats subjected to heat treatment above the glass transition temperature (*T_g*) but below the melting point (*T_m*),⁴⁸ further supporting TFC fabrication.

Green TFC membrane fabrication

The free-standing selective layers were synthesized using various monomer concentrations to investigate the reactivity of the novel green genipin-priamine monomer system (section S10 in the ESI†).

The preliminary experiments were conducted by forming a free-standing selective layer using a genipin concentration of 0.5 w/v% and a priamine concentration of 2 w/v%. The free-standing selective layer was observed at the interface after 10 min; therefore, the IP reaction time was set as 10 min for further investigation. Moreover, citric acid (0.1 w/v%) was used to adjust the pH of the aqueous solution (slight acidic) in the fabrication of all the membranes; therefore, only genipin and priamine concentrations were altered during membrane synthesis. Gelatin aqueous solution was used to form the interlayer on the h-PLA support (section S6 in the ESI†), and no significant morphology change was observed in the SEM images after the interlayer fabrication (section S6 in the ESI†).

The gelatin solution was prepared at 60 °C, and the high-concentration gelatin solution solidified at room temperature, likely causing defects in the final TFC membrane upon drying. To this end, we set the final gelatin concentration to be 2 w/v% for further membrane fabrication.

Fig. 3 shows the XPS, TGA, ATR, FT-IR, and the ¹³C SSNMR spectra and the chemical properties of the free-standing selective layer, while the detailed reaction scheme can be found in section S7 in the ESI†. Due to the presence of the ester group on the genipin molecule, the S_N2 nucleophilic substitution of an amine group is first observed during the cross-linking process.⁴⁹ Then, an intermediate aldehyde group is formed by an initial nucleophilic attack on genipin from a primary amine group. Subsequently, this aldehyde group is attacked by the secondary amine resulting from the previous step; therefore, the dihydropyran ring is opened.³⁷ Consequently, a heterocyclic compound of genipin linked to the priamine residue is formed. Slightly acidic media can have positive enhancement on the reaction, by making the ester group more susceptible to nucleophilic attack by the amine group, while driving forward the consecutive elimination step by protonation of the



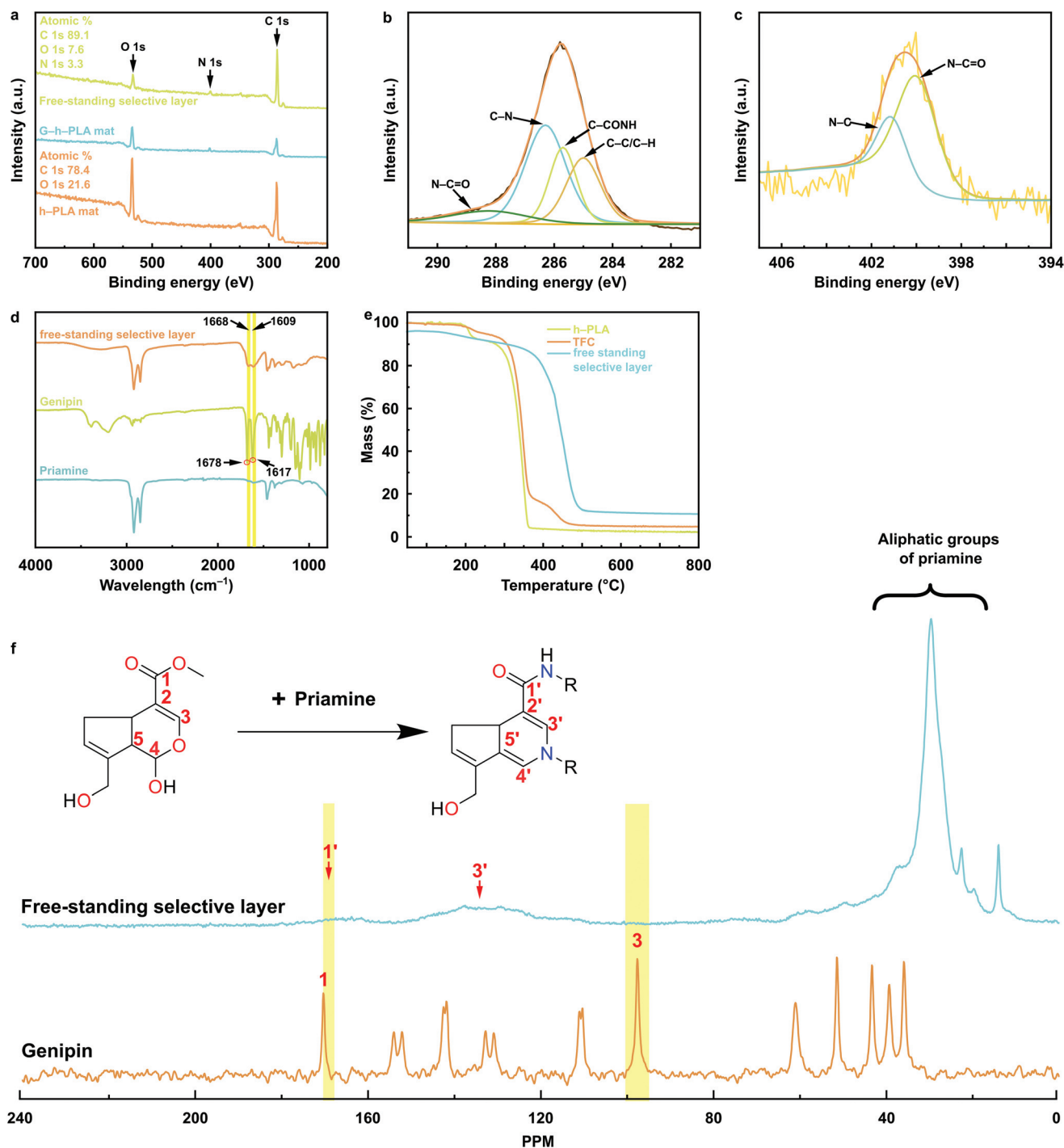


Fig. 3 Membrane fabrication mechanism and chemical characterizations: wide X-ray photoelectron spectroscopy (XPS) spectra of the green TFC free-standing selective layer and the h-PLA support (a) deconvoluted high-resolution C 1s (b) and N 1s (c) peaks, and (d) attenuated total-reflectance Fourier-transform infrared (ATR FT-IR) spectra, (e) TGA diagram of the TFC materials, and the reaction mechanism based on solid-state nuclear magnetic resonance (ssNMR) evaluation (f).

hydroxyl group. The optimal pH of the aqueous medium should be in the range when the protonation of the ester carbonyl group can occur, while retaining the nucleophilic nature of the primary amine species. To facilitate the crosslinking process between genipin and priamine, 0.1 w/v% citric acid was used as a green acid additive in the IP system. While both

intra- and inter-molecular crosslinking can occur, only the latter one results in a crosslinked network polymer and film formation. This can be confirmed by the appearance of a new N 1s peak as the result of the IP process (Fig. 3a), while the increase in the C/O ratio from 3.63 (h-PLA) to 11.7 (genipin/priamine selective layer) reflects the addition of long aliphatic

Table 1 Elemental composition of TFC membranes based on XPS

Membrane	Atomic composition (%)				Convolved peak percentages (%)			
	C	O	N	O/N ratio	N-C=O	C-N	C-CONH/C-COO	C-C/C-H
M6	78.26	19.45	2.29	8.49	17.36	30.04	31.97	20.63
M7	82.61	14.86	2.53	5.87	14.83	30.81	40.52	13.84
M8	81.24	15.99	2.78	5.75	13.76	26.58	43.79	15.86
M9	82.39	14.81	2.8	5.29	12.78	24.04	45.28	17.89
M2	89.09	7.61	3.31	2.30	10.39	25.79	46.44	17.37
M10	80.67	17.88	1.46	12.26	12.27	21.23	37.32	29.18
M11	78.27	20.09	1.64	12.25	11.84	22.46	43.26	22.45
M12	82.35	15.83	1.82	8.70	10.25	27.77	46.62	15.36
M13	81.76	16.08	2.16	7.44	10.19	28.04	47.09	14.67

chains from priamine. In particular, the deconvoluted four peaks from the C 1s high-resolution spectra can be found in Fig. 3b. The first peak corresponds to the C-H and C-C bonds at 285 eV, the second peak at 285.7 eV results from the β shift of strong electron-withdrawing groups, such as amide and carboxylic acid, which bond with the carbon atom (C-CONH, C-COO),⁵⁰ the third peak at 286.3 eV is related to the C-N bond, and a minor peak related to the N-C=O group is found at 288.2 eV.⁵¹ The N-C=O peak at 400.0 eV in Fig. 3c deconvoluted from the high-resolution N 1s spectra also proves the formation of amide between genipin and priamine.

Fig. 3d shows the FT-IR spectra of genipin, priamine, and the free-standing selective layer. Priamine revealed a characteristic peak from 2700 to 3000 cm^{-1} , corresponding to the aliphatic C-H stretching bond. Genipin showed a broad peak located in the range of 2000–3700 cm^{-1} due to the presence of the -OH group and hydrogen bonding. In addition, the two sharp peaks at 1678 and 1617 cm^{-1} were associated with the C=C stretching bond. The new peak at 1668 cm^{-1} observed from the free-standing selective layer was attributed to the amide group, which corresponds to C=O stretching deformation vibrations. The peak at 1609 cm^{-1} corresponds to the aromatic amide N-H deformation vibrations. The FT-IR spectra confirmed the formation of the polyamide structure of the TFC membrane. The starting (5% loss) thermal decomposition temperature of the h-PLA mat was 211.2 °C and that of the free-standing selective layer was 283.5 °C (Fig. 3e). By coupling these two polymers, our TFC exhibited a thermal decomposition temperature that started at 248.7 °C, indicating the successful fabrication of the composite membrane.

The slight shift of the resonance peak of the carbon atom C1 of genipin from 167.2 to 168.7 ppm indicated that the ester substitution occurred on genipin (Fig. 3f), while the significant shift of the carbon atom C4 peak from 100 ppm to the olefinic carbon atom at 131 ppm proved the formation of a double bond on the six-member ring. These observations support the two-step crosslinking reaction, which is typical for genipin.³⁷ First, a primary amine group is formed by the nucleophilic attack of the genipin C3 carbon atom, leading to dihydropyran ring opening; second, the resulting aldehyde group is attacked by the free amine groups, thereby forming the secondary amine (refer to section S7 in the ESI†). In

addition, the aliphatic peaks of priamine are detected in the range of 14–43 ppm on the free-standing selective layer, showing the successful coupling of priamine onto genipin.

We evaluated the carbon, oxygen, and nitrogen content in the TFC membranes, including the convoluted C 1s peaks for all the membranes with different monomer concentrations (Table 1 and section S8 in the ESI†). The extent of genipin cross-linking was estimated from the relative atomic concentrations of N and O measured using XPS. The fully cross-linked structure requires the substitution of both the oxygen atom in the six-membered heterocycle, and the oxygen atom in the ester group of the genipin molecule to the nitrogen atom from priamine; hence, two oxygen atoms correspond to two nitrogen atoms.³⁷

However, the fully linear structure leaves the ester group unreacted, resulting in three oxygen atoms corresponding to one nitrogen atom. Therefore, a small O/N ratio resulted in a low degree of cross-linking between genipin and priamine.

As shown in Table 1, all TFC membranes belonged to low-N-content membranes as the N percentage of the membrane was lower than 10%.⁵² In addition, as the concentration of genipin increased from 0.1 w/v% to 0.5 w/v%, the O/N ratio decreased from 8.49 to 2.29. Similarly, a decreasing trend in the O/N ratio was observed as the concentration increased, indicating the cross-linking structure was enhanced by the increased monomer concentrations. We also deconvoluted the C 1s peaks into four peaks, refer to section S8 in the ESI†. An increasing trend can be found under the peak at 285.7 eV (C-CONH/C-COO) as the concentration of genipin increased from 0.1 w/v% to 0.5 w/v%, indicating that the content of the cross-linked amide structure increased accordingly (from 31.97% to 46.44%). Similarly, the increasing priamine concentration enhanced the IP process as the percentage of the C-CONH/C-COO peak elevated from 37.32% (priamine at 0.5 w/v%) to 47.09% (priamine at 2.5 w/v%). Since the priamine 1071 used in this project was a mixture of amines with different carbon chain lengths (refer to section S9 in the ESI†), the percentage of the C-C/C-H peak was not considered as a precise descriptor of the cross-linking degree.

Fig. 4 reveals the characteristics of the TFC membrane. The defect-free free-standing selective layer was formed on the electrospun nanofibrous PLA support (Fig. 4a and b). The syn-



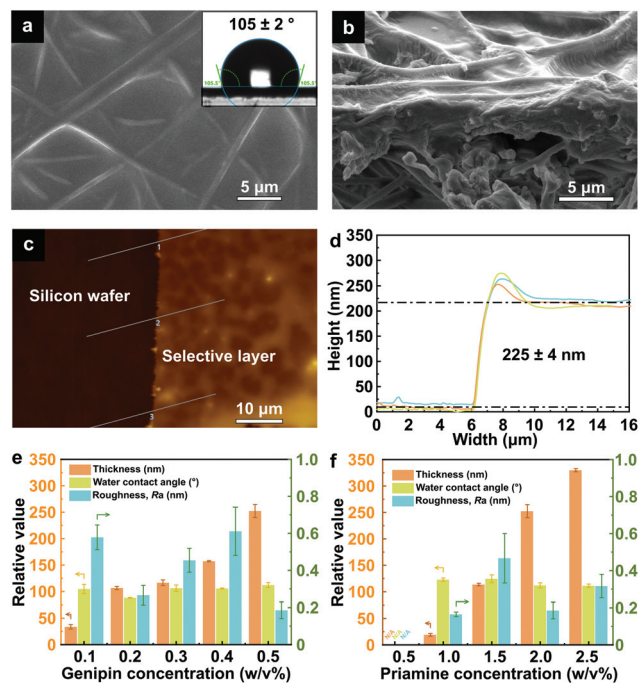


Fig. 4 SEM image and water contact angle (inset) of the surface of green TFC membrane fabricated from 0.5 w/v% genipin aqueous solution and 2 w/v% priamine–eucalyptol system (a) and the corresponding cross-sectional image (b). The inset shows the water contact angle. AFM thickness detection (c), and measurement (d) of the thin film made from 0.5 w/v% genipin aqueous solution and 2 w/v% priamine–eucalyptol system and the thickness, roughness, and water contact angle measurements of green TFC membranes under various genipin (e) and priamine concentrations (f).

thesized TFC membrane was hydrophobic with a water contact angle of $105^\circ \pm 2^\circ$, indicating the incorporation of priamine with long aliphatic chains. The thickness of the free-standing selective layer was measured to be approximately 225 nm based on AFM analysis (Fig. 4c and d).

The free-standing selective layer thickness, surface roughness, and WCA are key factors that influence the OSN performance; therefore, we studied the correlation between membrane properties and performance by altering the reaction parameters of IP (Fig. 4e and f).

The detailed SEM images of the surface and the cross section as well as the AFM 3D morphology of each TFC membrane are provided in section S10 in the ESI†. As the concentration of genipin increased from 0.1 to 0.5 w/v%, the thickness of the free-standing selective layer increased from approximately 30 to 225 nm. Similarly, the thickness increased from 25 to 325 nm when the concentration of priamine increased from 1 to 2.5 w/v%. No selective layer was formed when the priamine concentration was as low as 0.5 w/v%.

The WCA, which fell between 88° and 125° (Fig. 4e and f), was not significantly affected by the change in monomer concentrations. All the TFC membranes exhibited a WCA higher than 90° , which reflects increased hydrophobicity after the incorporation of the long aliphatic chains of priamine.⁷

The support with the interlayer showed a WCA between that of the pure PLA and gelatin. Owing to the incorporation of the gelatin interlayer, the hydrophilicity of the electrospun PLA support decreased from approximately 0° to 23° (section S10 in the ESI†) due to the less hydrophilic nature of gelatin (WCA = 58° for the dense film) compared to PLA (WCA = 56° for the dense film).

Membrane performance

The rejection of different molecules increased as the result of the increased priamine concentration (Fig. 5a), while the acetone permeance decreased from 55.2 to $6.8 \text{ L m}^{-2} \text{ h}^{-1} \text{ bar}^{-1}$ (Fig. 5b). As the membranes got tighter (M10 → M13), the MWCO decreased to 176 g mol^{-1} . There was no selective layer at a low priamine concentration of 0.5 w/v% (M10), which led to the uneven distribution of the polyamide structure (refer to section S15 in the ESI†); hence, all the rejections were lower than 90% (Fig. 5a). Similarly, the pore sizes of the prepared TFC membranes were all comparatively small; as the concentration of priamine increased from 1 to 2.5 w/v%, the mean pore diameter decreased from 0.9 nm to 0.5 nm (Fig. 5c). These results are in line with the previous findings, indicating that a denser selective layer was formed under a higher monomer concentration; therefore, a tighter membrane with a lower MWCO and acetone permeance was obtained.

The permeance through the green TFC membrane prepared using 0.5 w/v% genipin and 2 w/v% priamine concentrations (M2) was evaluated using pure solvents, including toluene, EtOH, MEK, acetone, and MeCN, as they cover a wide range of solvent polarity, and the h-PLA support was found to be stable in these solvents (refer to section S2 in the ESI†). The filtration was conducted under 30 bar. A linear correlation ($R^2 = 0.9992$) between the permeance and the solubility parameter (Fig. 5d), which comprises the solvent solubility ($\delta_{p,s}$), viscosity (η), and molar diameter ($d_{m,s}$) (refer to section S12 in the ESI†), was found. To further investigate the effect of pressure on the membrane performance, the applied pressure was varied between 10 and 30 bar with 5-bar increments using M2 in different solvents (Fig. 5e). A linear increase in flux as a function of pressure was observed for all solvents, proving that the pressure difference is the only driving force for solvent permeation,⁵³ and no compaction of the synthesized membrane occurred during the operation even under a pressure as high as 30 bar.⁵⁴ MeCN has the highest polarity among the solvents used, which resulted in a lower solubility in the hydrophobic surface of the selective layer. Nevertheless, MeCN was more permeable at high pressure due to its low viscosity and smallest molar diameter, resulting in the highest slope (Fig. 5e). In addition, the durability of the selective layer at the highest operating pressure (30 bar) was demonstrated.

To demonstrate the industrial feasibility of the synthesized green TFC membranes, their long-term stability performance in acetone was evaluated using a crossflow nanofiltration rig under continuous operation for over 7 days (Fig. 5f). The initial acetone permeance was estimated to be



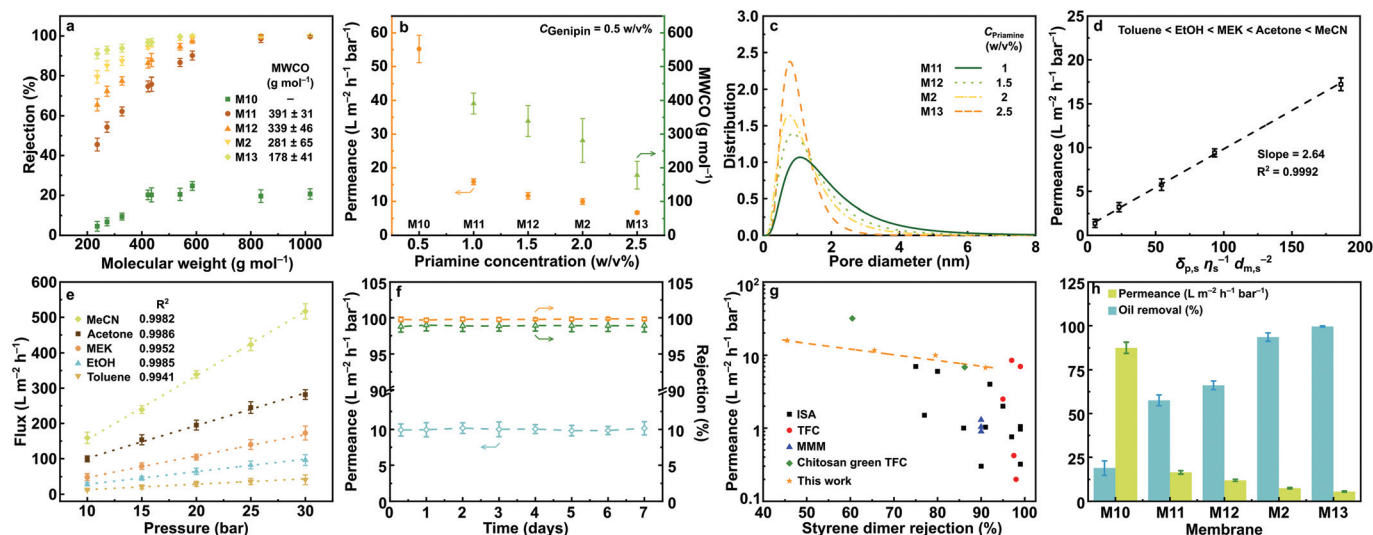


Fig. 5 Green TFC membrane performance: (a) rejection profiles of the membranes; (b) permeance and MWCO values of the membranes fabricated under different priamine concentrations at fixed C_{Genipin} (0.5 w/v%); (c) pore size distribution with different priamine concentrations; (d) pure solvent permeance as a function of the solubility parameter for M2; (e) pure solvent flux as a function of pressure for M2; (f) long-term performance testing of M2 under continuous crossflow operation; (g) permeance versus styrene dimer rejection (235 g mol⁻¹) of our membranes compared with the reported values in the literature (section S14 in the ESI†); (h) oil-in-water emulsion separation performance (section S13 in the ESI†). All filtrations were performed in acetone at 30 bar unless stated otherwise.

9.9 L m⁻² h⁻¹ bar⁻¹ with 99% of oleuropein and 100% of acid fuchsin rejection. The membrane exhibited a stable steady-state performance over the 7 days of continuous operation. To assess the separation performance of the green TFC membranes, their acetone permeance and styrene dimer rejection were compared with those of mixed matrix membranes, ISA membranes, and TFC membranes reported in the literature (Fig. 5g, section S14 in the ESI†).

The green TFC membranes fabricated with different priamine concentrations exhibited a general rejection-permeance trade-off. The acetone permeance was among the highest, while the styrene dimer rejection was comparable to those of the current membranes.

Interestingly, the change in priamine concentration significantly affected the styrene dimer rejection in the range of 45% and 91%, while the acetone permeance changed from 16 to 7 L m⁻² h⁻¹ bar⁻¹.

The membranes were also subjected to oil-in-water emulsion separation (Fig. 5h, section S13 in the ESI†). The M10 membrane with the lowest priamine concentration (0.5 w/v%) showed the highest water permeance of 87.5 L m⁻² h⁻¹ bar⁻¹ with low oil removal efficiency (19%), caused by the uneven distribution of the polyamide layer (section S10 in the ESI†). The observed low oil separation performance of M10 is in line with the low OSN performance (Fig. 5a). With the increase in the priamine concentration to 2.5 w/v%, the M13 membrane exhibited excellent performance with an oil removal efficiency of 99.6% and a water permeance of 5.6 L m⁻² h⁻¹ bar⁻¹. Overall, the outstanding performance and the long-term stability demonstrated the potential of green TFC membranes to replace petroleum-based membranes in OSN and oil separation applications. Note that PLA is a polyester

that can undergo alcoholysis, and such conditions should be avoided to avoid degradation of the support.

Sustainability evaluation

Our green membrane fabrication system utilized sustainable materials and green solvents from the macro- to the nano-scale. The biodegradable biopolymer PLA was used to prepare a nanofibrous membrane support in DMC with a scalable and green electrospinning technology.^{55,56} The compatibility between the support and the selective layer was achieved through the deposition of an interlayer using an aqueous solution of gelatin, which is derived from fish scales and is considered biocompatible and fully biodegradable. Plant-derived genipin and priamine were used as green monomers in water and eucalyptol to obtain the selective layer of the TFC membrane. This is the first reported TFC membrane fabrication system that does not rely on any fossil-based chemicals. To compare the sustainability of our TFC membrane fabrication system with previous approaches, the chemicals in the selective layer were calculated with their molar numbers (Fig. 6).

The total mole number of chemicals consumed in our green TFC membrane fabrication ranged from 1.5 to 3.1 mmol, while it was 2.7 mmol for the M2 membrane with the optimum monomer concentration. The conventional petroleum-based TFC membranes composed of MPD and TMC used up to 12 mmol of chemicals, while the total molar number can be as high as 87 mmol in extreme cases (Fig. 6a, section S15 in the ESI†). Owing to the efforts in sustainable membrane fabrication, these values were significantly low for green TFC systems (Fig. 6b). However, MPD or TMC were still used for green membrane fabrication, and exceptionally green



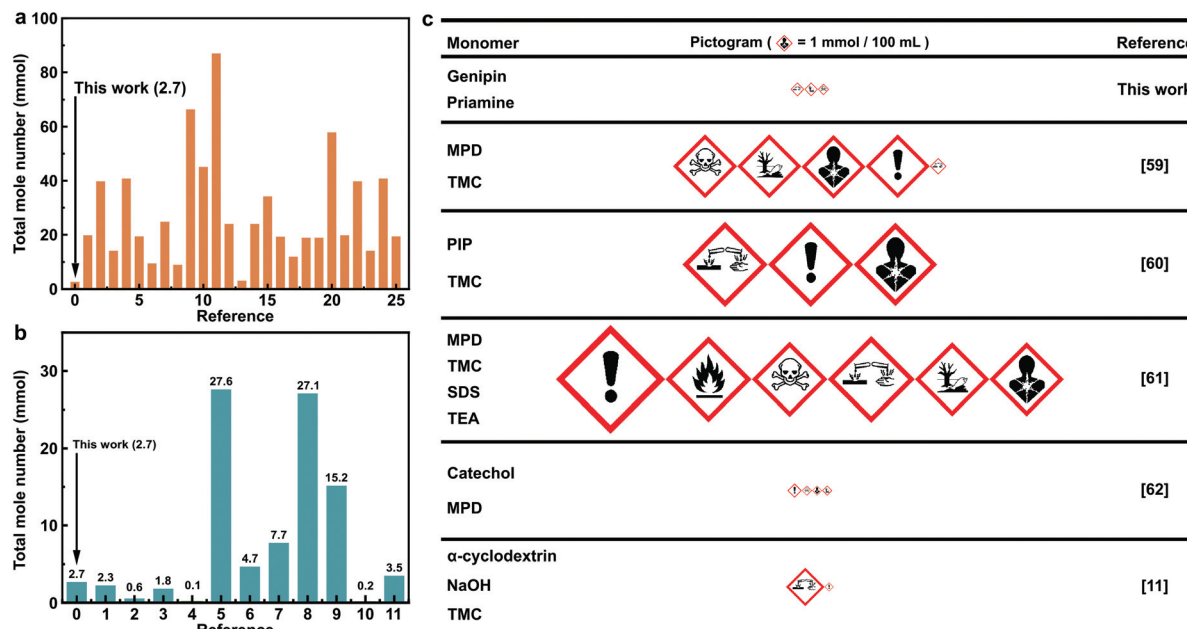


Fig. 6 Sustainability analysis of TFC membrane fabrication. Total mole number of the used monomers and additives in the IP process for (a) petroleum-based TFC membranes (section S15 in the ESI†) and (b) green TFC membranes (section S15 in the ESI†). Refer to the ESI† for the details. (c) Chemical hazards and toxicity related to TFC membranes. The area of a pictogram is proportional to the total mole number of the corresponding chemical used. The references in (a) and (b) can be found in the corresponding tables in ESI†, while the cited works in (c) can be found in the reference list of the main article.

TFC membrane fabrication appeared in two recent studies.^{7,8} Among all the green TFC membranes, six of them had higher total mole numbers, whereas three of them were comparable to ours.

According to the Globally Harmonized System of Classification and Labelling of Chemicals, the hazard and toxicity related to the IP reaction were represented by pictograms in Fig. 6c. Considering the total number of moles, the pictogram size of each component was calculated, as shown in section S15 in the ESI†. In general, our proposed green TFC fabrication system has a smaller amount of chemical consumption as well as smaller pictograms compared to the existing petroleum-based and green TFC systems.

Besides the chemicals used in the selective layer, the biodegradable green PLA nanofibrous support further improved the sustainability of the genipin/priamine TFC membrane by avoiding hazardous and harsh solvents.

Meanwhile, the waste membrane disposal problem was solved without using additional organic solvents or dangerous chemicals. The presented TFC fabrication methodology takes us a step closer to achieving cradle-to-grave sustainable-membrane fabrication, which is among the recent grand challenges in the field.^{57,58}

We encourage future research on the solvent volume and the monomer concentration per unit membrane area to improve accuracy when evaluating sustainability. A direct and straightforward comparison between various studies can also contribute to sustainable membrane research and development.

Experimental

Materials and reagents

PLA provided by NatureWorks Ingeo 4043D and dimethyl carbonate (DMC, 99%) obtained from Alfa Aesar were used to prepare polymer solutions. Tetrabutylammonium bromide (TBAB, 99%), received from Sigma Aldrich, was used as the salt additive to enhance electrospinnability. Proteinase K (fungal) was obtained from Thermo Fisher Scientific and stored under -4°C . Genipin (98%), purchased from Guangzhou Jsen Trading Co., Ltd; priamine 1071, a dimer diamine, produced by Croda, the Netherlands; and eucalyptol (99%), and citric acid (99.5%) received from Sigma Aldrich were used. Hexadecyltrimethylammonium bromide (CTAB) was purchased from Acros Organics. All chemicals were used as received. Type II deionized water with a resistivity of $18.2\text{ M}\Omega\text{ cm}$ at 25°C (Milli-Q) was used in all the experiments.

Characterizations

The morphology of the electrospun nanofibers was observed by scanning electron microscopy (SEM) (Quattro SEM, FEI and Magellan SEM, FEI). Before SEM analysis, the fiber specimens were coated with 4 nm Pt using a sputtering system. The diameter distribution of the electrospun nanofibers was measured from the respective SEM images over approximately 100 nanofibers by ImageJ software (US National Institutes of Health, NIH). Atomic force microscope (AFM) in the tapping mode using a cantilever (RTESPA, Bruker) with a scan area of $20\text{ }\mu\text{m} \times 20\text{ }\mu\text{m}$ and a scan rate of 0.7 Hz was employed to



investigate the surface roughness of the membranes. Three different positions on each sample surface were scanned to obtain average arithmetic roughness (R_a) values with standard deviations. Water contact angle (WCA) measurements were performed on a drop shape analyzer (Krüss GmPh) in triplicate. Dynamic mechanical analysis (DMA) was conducted on TA Instruments Q800, and the data were obtained with standard deviations. Attenuated total-reflectance Fourier-transform infrared (ATR FT-IR, Nicolet iS10, Thermo Fisher Scientific) spectroscopy was used to investigate the chemical functional groups of the film and the bonding shifts of the monomers. X-ray photoelectron spectroscopy (XPS) analysis was performed on an Amicus instrument (Kratos Analytical, UK) using an achromatic Al X-ray source ($h\nu = 1486.6$ eV) operating at a power of 50 W under ultrahigh vacuum conditions and 10^{-9} mbar. The wide and narrow scan spectra were acquired at fixed analyzer pass energy (75 eV). The narrow scanning spectra were deconvoluted using XPSpeak41 software; peak values were initially input, and consequently, automatic peak fitting was optimized until no further change was noticed. One-dimensional ^{13}C CP/MAS solid-state nuclear magnetic resonance (ssNMR) spectra were recorded on a 400 MHz Bruker AVANCE III spectrometer, and the following sequence was used: 90 pulses on the proton (pulse length: 2.4 s), followed by a cross-polarization step with a contact time of typically 2 ms, and finally, the acquisition of the ^{13}C NMR signal under high-power proton decoupling. The delay between the scans was set to 5 s to allow the complete relaxation of the ^1H nuclei; the number of scans ranged from 3000 to 10 000. An exponential apodization function corresponding to a line broadening of 80 Hz was applied prior to the Fourier transformation. Thermal gravimetric analysis (TGA) was conducted using a TGA Q5000 (TA Instruments); all analyses entailed a ramping process with a speed of $5\text{ }^\circ\text{C min}^{-1}$ up to $800\text{ }^\circ\text{C}$. The pore size calculation can be found in the ESI.†

Electrospinning of the nanofibrous PLA support

PLA at concentrations of 5–15 w/v% and TBAB at concentrations of 1–15 w/w% (with respect to PLA content) were dissolved in DMC with continuous stirring under $60\text{ }^\circ\text{C}$ for 12 h (Table 2). The solution was then transferred into a 3 mL disposable plastic syringe (Normjet™ Thermo Scientific) equipped with a blunt metallic needle (Tyco, Kendall 26G). The syringe was placed on a syringe pump (KD Scientific-Legato) and discharged at a speed of 0.5 mL h^{-1} . A high-power voltage supply (SRS, Stanford Research System) set to be 15 kV was used, and the tip-to-collector distance (TCD) was kept at 100 mm. The nanofibers were collected on a metal collector covered with an aluminum foil. During the electrospinning process, the temperature was maintained at $21\text{ }^\circ\text{C}$, and the relative humidity was in the range of 50%–55%.

10 mL of the polymer solution was used to produce a $150\text{ mm} \times 150\text{ mm}$ mat, followed by hot annealing under $100\text{ }^\circ\text{C}$ for 12 h to enhance the mechanical properties of the PLA support. The annealed PLA mat is hereafter referred to as h-PLA.

Table 2 Electrospun nanofibrous PLA TFC membrane supports

Support	C_{PLA} (w/v%)	C_{TBAB} (w/w%)	Voltage (kV)	Flow rate (mL h^{-1})	TCD (mm)
S1	5	0	15	0.5	100
S2	7.5	0	15	0.5	100
S3	10	0	15	0.5	100
S4	12.5	0	15	0.5	100
S5	15	0	15	0.5	100
S6	12.5	1	15	0.5	100
S7	12.5	2.5	15	0.5	100
S8	12.5	5	15	0.5	100
S9	12.5	7.5	15	0.5	100
S10	12.5	10	15	0.5	100
S11	12.5	10	10	0.5	100
S12	12.5	10	12.5	0.5	100
S13	12.5	10	15	0.5	100
S14	12.5	10	17.5	0.5	100
S15	12.5	10	20	0.5	100
S16	12.5	10	15	0.25	100
S17	12.5	10	15	0.5	100
S18	12.5	10	15	1	100
S19	12.5	10	15	2	100
S20	12.5	10	15	0.5	50
S21	12.5	10	15	0.5	100
S22	12.5	10	15	0.5	150
S23	12.5	10	15	0.5	200

Swelling testing

The swelling test of the h-PLA support and the selective layer was conducted by obtaining the dry and wet weight of the films ($10 \times 10\text{ mm}$), according to eqn (1). The films were immersed in given solvents for 24 h before measuring their wet weight. The experiments were performed in triplicates.

$$R_s = \frac{m_{\text{wet}} - m_{\text{dry}}}{m_{\text{dry}}} \times 100\% \quad (1)$$

Biodegradation of the nanofibrous PLA support

The h-PLA supports were cut into $15 \times 15\text{ mm}$ pieces and placed in a Petri dish with a diameter of 30 mm.

Consequently, 3 mL $200\text{ }\mu\text{g mL}^{-1}$ proteinase K in 0.05 M Tris buffer solution (pH = 8) was added to the Petri dish. All the samples were kept under $37\text{ }^\circ\text{C}$, and digital photos were taken periodically.

Preparation of genipin–priamine TFC membranes

Membranes were prepared using various interlayer and monomer concentrations (Table 3). The genipin–priamine free-standing selective layer was prepared to study the chemical structure of the polyamide layer. The fabrication was conducted in a 20 mL glass vial containing 5 mL 0.5 w/v% genipin aqueous solution with 0.1 w/v% citric acid and 5 mL 2 w/v% priamine in eucalyptol.

The gelation interlayer was prepared by pouring 5 mL 2 w/v% aqueous gelatin solution into a 25 cm^2 h-PLA mounted gasket for 0.5 h under $60\text{ }^\circ\text{C}$; consequently, the excess liquid was decanted, and the residue gelatin solution was removed using an air knife for 1 min. Another 5 mL 0.5 w/v% genipin solution was added subsequently, and the mat was kept under



Table 3 Membrane fabrication at various interlayer and monomer concentrations. The solvent for the gelatin interlayer, 0.1 w/v% aq. citric acid, and the genipin aqueous phase was water, and it was eucalyptol for the priamine organic phase

Membrane	C_{gelatin} (w/v%)	C_{genipin} (w/v%)	C_{priamine} (w/v%)
M1	1	0.5	2
M2	2	0.5	2
M3	3	0.5	2
M4	4	0.5	2
M5	5	0.5	2
M6	2	0.1	2
M7	2	0.2	2
M8	2	0.3	2
M9	2	0.4	2
M10	2	0.5	0.5
M11	2	0.5	1
M12	2	0.5	1.5
M13	2	0.5	2.5

37 °C for 0.5 h. Hereafter, the prepared support is referred to as G-h-PLA. After the deposition of the interlayer, the green TFC membrane was synthesized *via* the IP reaction between genipin and priamine on the G-h-PLA support.

First, 5 mL 0.5 w/v% genipin solution containing 0.1 w/v% citric acid was poured onto the prepared G-h-PLA for 5 min at room temperature (22 ± 1 °C). Then, the excess aqueous solution was decanted. Next, 5 mL priamine in eucalyptol was immediately added into the system, where the organic solution was allowed to react for 10 min to form the selective layer on the support. The prepared TFC membranes were washed with pure eucalyptol thrice and then stored in water.

Nanofiltration

The OSN performance of the TFC membranes was evaluated using a crossflow membrane separation rig. An ATEX-rated gear pump manufactured by MSE Ltd (UK) was used for the recirculation of the retentate stream set to 1200 mL min⁻¹. The membranes were rinsed with the filtration solvent and then stored in the solvent for 16 h before filtration.

To reach a steady-state operation, the membranes were conditioned under the given pressure for 24 h prior to the permeance and rejection measurements.

The permeance was obtained by measuring the permeate volume (V) over a given time (t) period for the given membrane area ($A = 28$ cm²) and applied pressure.

$$\text{Permeance [L m}^{-2} \text{ h}^{-1} \text{ bar}^{-1}] = \frac{J}{\Delta P} = \frac{V}{\Delta P \times A \times t} \quad (2)$$

The rejection profiles were determined from the ratio of the permeate (c_{permeate}) and retentate ($c_{\text{retentate}}$) concentrations of the solutes using eqn (3). Various marker dyes and pharmaceuticals, namely styrene dimer ($M_w = 236$ g mol⁻¹), estradiol ($M_w = 272$ g mol⁻¹), methyl orange ($M_w = 327$ g mol⁻¹), losartan ($M_w = 423$ g mol⁻¹), valsartan ($M_w = 435.42$ g mol⁻¹), oleuropein ($M_w = 540.51$ g mol⁻¹), acid fuchsin ($M_w = 585.54$ g mol⁻¹), roxithromycin ($M_w = 837$ g mol⁻¹), and rose bengal ($M_w = 1018$ g mol⁻¹) solutes were dissolved in acetone and

used for filtration. The molecular weight cut-off (MWCO), defined as the lowest molecular weight of a solute that is 90% retained by the membrane, was estimated from the rejection curves by nonlinear interpolation. Two independent measurements were performed on independently prepared membranes; the standard deviations were reported in the figures as error bars.

$$\text{Rejection [\%]} = \left(1 - \frac{c_{\text{permeate}}}{c_{\text{retentate}}}\right) \times 100. \quad (3)$$

The long-term stability of M2 was assessed under the conditions described above using oleuropein and acid fuchsin markers in acetone. The crossflow nanofiltration rig was operated continuously over 7 days. CTAB was used as an emulsifier to prepare oil-in-water emulsions, as simulated produced water with a high mechanical shearing rate. Approximately 0.5 g vegetable oil (0.5 g L⁻¹), 50 mg CTAB, and 1 L water were mixed by T-18 ULTRA-TURRAX (IKA England Ltd) at 15 000 rpm for 120 s at 21 °C to prepare the feed solution.

The stability of the green TFC membrane was evaluated by placing M2 membrane pieces (0.5 × 0.5 cm) in 4 mL of various solvents, including vegetable oil and aqueous solutions with different pH levels, at room temperature in closed vials for up to 30 days using gentle agitation in an IKA incubator shaker operated at 100 rpm.

Conclusions

A green TFC membrane comprising natural monomers genipin and priamine was successfully fabricated through IP. Eucalyptol was used as a green solvent for the organic phase. PLA, a biodegradable natural polymer, was electrospun into a nanofibrous mat, which was used as a highly porous support for the TFC membrane. The robustness of the fabricated PLA support was enhanced by hot annealing, as the tensile strength and Young's modulus of the support increased from 1.62 to 4.55 MPa and from 25.36 to 60.12 MPa, respectively. The nanofibrous PLA support was fully biodegraded by proteinase K within 10 h, making the waste membrane disposal mild and green. A gelatin interlayer between the PLA support and the selective layer was utilized to improve the compatibility of these two layers. The formation of the solvent-resistant selective layer was promoted by the addition of citric acid as a green acid catalyst in the aqueous phase. After that, the reaction conditions were altered by changing the genipin and priamine concentrations to obtain a high acetone permeance (10 L m⁻² h⁻¹ bar⁻¹) and low MWCO (281 g mol⁻¹). The prepared green TFC membrane also exhibited excellent oil removal efficiency (99.6%) with a water permeance of 5.6 L m⁻² h⁻¹ bar⁻¹, indicating that our membrane can be applied to separate solutes under both organic and aqueous environments and can withstand both oils and organic solvents. Ultimately, we created a highly permeable green TFC membrane with comparable styrene dimer rejection among the various membranes reported in the literature. The green TFC membrane exhibited



a long-term, steady separation performance over seven days of continuous cross-flow filtration under 30 bar. The proposed fully degradable TFC membrane fabrication system was based solely on the use of sustainable raw materials and green solvents. The synthesized TFC membranes maintained outstanding sustainability without compromising performance, manifesting themselves as environmentally benign sustainable solutions for molecular separations in organic media.

Conflicts of interest

There are no conflicts to declare.

Acknowledgements

Fig. 1 and the graphical abstract were created by Xavier Pita, scientific illustrator at the King Abdullah University of Science and Technology (KAUST). The research reported in this publication was supported by funding from KAUST.

References

- H. A. Le Phuong, C. F. Blanford and G. Szekely, *Green Chem.*, 2020, **22**, 3397–3409.
- P. Marchetti, M. F. Jimenez Solomon, G. Szekely and A. G. Livingston, *Chem. Rev.*, 2014, **114**, 10735–10806.
- Y. Li, Z. Guo, S. Li and B. Van der Bruggen, *Adv. Mater. Interfaces*, 2021, **8**, 2001671.
- D. Zou, S. P. Nunes, I. F. J. Vankelecom, A. Figoli and Y. M. Lee, *Green Chem.*, 2021, **23**, 9815–9843.
- W. Xie, T. Li, A. Tiraferri, E. Drioli, A. Figoli, J. C. Crittenden and B. Liu, *ACS Sustainable Chem. Eng.*, 2021, **9**, 50–75.
- C. Ong, G. Falca, T. Huang, J. Liu, P. Manchanda, S. Chisca and S. P. Nunes, *ACS Sustainable Chem. Eng.*, 2020, **8**, 11541–11548.
- S.-H. Park, A. Alammar, Z. Fulop, B. A. Pulido, S. P. Nunes and G. Szekely, *Green Chem.*, 2021, **23**, 1175–1184.
- S.-H. Park, C. Yang, N. Ayaril and G. Szekely, *ACS Sustainable Chem. Eng.*, 2022, **10**, 998–1007.
- X. Jiang, W. F. Yong, J. Gao, D.-D. Shao and S.-P. Sun, *J. Membr. Sci.*, 2021, **635**, 119530.
- M. H. Abdellah, L. Pérez-Manríquez, T. Puspasari, C. A. Scholes, S. E. Kentish and K.-V. Peinemann, *Adv. Sustainable Syst.*, 2018, **2**, 1800043.
- M. H. Abdellah, L. Pérez-Manríquez, T. Puspasari, C. A. Scholes, S. E. Kentish and K.-V. Peinemann, *J. Membr. Sci.*, 2018, **567**, 139–145.
- D. Hua, S. Japip, K. Y. Wang and T.-S. Chung, *ACS Sustainable Chem. Eng.*, 2018, **6**, 10696–10705.
- C. Han, H. Liu and Y. Wang, *J. Membr. Sci.*, 2022, **644**, 120192.
- N. Horzum, R. Muñoz-Espí, M. A. Hood, M. M. Demir and D. Crespy, *Green Electrospinning*, De Gruyter, ed. N. Horzum, M. M. Demir, R. Muñoz-Espí and D. Crespy, 2019, pp. 11–40.
- Y. Li, E. Wong, A. Volodine, C. Van Haesendonck, K. Zhang and B. Van der Bruggen, *J. Mater. Chem. A*, 2019, **7**, 19269–19279.
- T.-D. Lu, B.-Z. Chen, J. Wang, T.-Z. Jia, X.-L. Cao, Y. Wang, W. Xing, C. H. Lau and S.-P. Sun, *J. Mater. Chem. A*, 2018, **6**, 15047–15056.
- C. Han, X. Zhang, C. Ding, S. Xiong, X. Yu and Y. Wang, *J. Membr. Sci.*, 2020, **612**, 118447.
- X. You, J. Y. Chong, K. S. Goh, M. Tian, J. W. Chew and R. Wang, *J. Membr. Sci.*, 2021, **640**, 119825.
- L. Shen, Q. Shi, S. Zhang, J. Gao, C. Cheng David, M. Yi, R. Song, L. Wang, J. Jiang, R. Karnik and S. Zhang, *Sci. Adv.*, 2021, **7**, eabg6263.
- C. Han, Q. Liu, Q. Xia and Y. Wang, *J. Membr. Sci.*, 2022, **641**, 119911.
- T.-D. Lu, L.-L. Zhao, W. F. Yong, Q. Wang, L. Duan and S.-P. Sun, *Chem. Eng. J.*, 2021, **409**, 128206.
- X. Li, S. Gong, L. Yang, F. Zhang, L. Xie, Z. Luo, X. Xia and J. Wang, *Polymer*, 2020, **188**, 121991.
- J. Chen, L. Lu, D. Wu, L. Yuan, M. Zhang, J. Hua and J. Xu, *ACS Sustainable Chem. Eng.*, 2014, **2**, 2102–2110.
- H. A. Le Phuong, N. A. Izzati Ayob, C. F. Blanford, N. F. Mohammad Rawi and G. Szekely, *ACS Sustainable Chem. Eng.*, 2019, **7**, 11885–11893.
- F. Imani, R. Karimi-Soflou, I. Shabani and A. Karkhaneh, *Polymer*, 2021, **218**, 123487.
- A. Wagner, V. Poursorkhabi, A. K. Mohanty and M. Misra, *ACS Sustainable Chem. Eng.*, 2014, **2**, 1976–1982.
- S. Sato, D. Gondo, T. Wada, S. Kanehashi and K. Nagai, *J. Appl. Polym. Sci.*, 2013, **129**, 1607–1617.
- M. Pierpaoli, C. Giosuè, N. Czerwińska, M. Ryciewicz, A. Wieloszyńska, R. Bogdanowicz and M. L. Ruello, *Materials*, 2021, **14**, 6766.
- G. Fiorani, A. Perosa and M. Selva, *Green Chem.*, 2018, **20**, 288–322.
- M. A. Abdullah, H. A. Hussein and O. M. S. Alshajrawi, in *Green Sustainable Process for Chemical and Environmental Engineering and Science*, ed. Inamuddin, A. M. Asiri and S. Kanchi, Elsevier, 2021, pp. 185–194.
- D. D. da Silva Parize, M. M. Foschini, J. E. de Oliveira, A. P. Klamczynski, G. M. Glenn, J. M. Marconcini and L. H. C. Mattoso, *J. Mater. Sci.*, 2016, **51**, 4627–4638.
- H. Mokarizadeh, S. Moayedfard, M. S. Maleh, S. I. G. P. Mohamed, S. Nejati and M. R. Esfahani, *Sep. Purif. Technol.*, 2022, **278**, 119451.
- X.-Y. Chi, B.-G. Xia, Z.-L. Xu and M.-X. Zhang, *ACS Omega*, 2018, **3**, 13009–13019.
- W. Wu, L. Yu, L. Li, Z. Li, J. Kang, S. Pu, D. Chen, R. Ma, K. An, G. Liu and Y. Yu, *Desalination*, 2021, **518**, 115283.
- K. Shen, C. Cheng, T. Zhang and X. Wang, *J. Membr. Sci.*, 2019, **588**, 117192.
- C. Pizzolitto, M. Cok, F. Asaro, F. Scognamiglio, E. Marsich, F. Lopez, I. Donati and P. Sacco, *Int. J. Mol. Sci.*, 2020, **21**, 6831.



- 37 M. F. Butler, Y.-F. Ng and P. D. A. Pudney, *J. Polym. Sci., Part A: Polym. Chem.*, 2003, **41**, 3941–3953.
- 38 C. Nunes, É. Maricato, Â. Cunha, M. A. M. Rocha, S. Santos, P. Ferreira, M. A. Silva, A. Rodrigues, O. Amado, J. Coimbra, D. Silva, A. Moreira, S. Mendo, J. A. Lopes da Silva, E. Pereira, S. M. Rocha and M. A. Coimbra, *Green Chem.*, 2016, **18**, 5331–5341.
- 39 M. Nair, R. K. Johal, S. W. Hamaia, S. M. Best and R. E. Cameron, *Biomaterials*, 2020, **254**, 120109.
- 40 M. Razali, J. F. Kim, M. Attfield, P. M. Budd, E. Drioli, Y. M. Lee and G. Szekely, *Green Chem.*, 2015, **17**, 5196–5205.
- 41 V. Hessel, N. N. Tran, M. R. Asrami, Q. D. Tran, N. Van Duc Long, M. Escribà-Gelonch, J. O. Tejada, S. Linke and K. Sundmacher, *Green Chem.*, 2022, **24**, 410–437.
- 42 J. H. Yu, S. V. Fridrikh and G. C. Rutledge, *Polymer*, 2006, **47**, 4789–4797.
- 43 H. Fong, I. Chun and D. H. Reneker, *Polymer*, 1999, **40**, 4585–4592.
- 44 F. Topuz, M. A. Abdulhamid, S. P. Nunes and G. Szekely, *Environ. Sci. Nano*, 2020, **7**, 1365–1372.
- 45 H. Maleki, A. A. Gharehaghaji, L. Moroni and P. J. Dijkstra, *Biofabrication*, 2013, **5**, 035014.
- 46 Q. Huang, M. Hiyama, T. Kabe, S. Kimura and T. Iwata, *Biomacromolecules*, 2020, **21**, 3301–3307.
- 47 S. Nauman, G. Lubineau and H. F. Alharbi, *Membranes*, 2021, **11**, 39.
- 48 E. P. S. Tan and C. T. Lim, *Nanotechnology*, 2006, **17**, 2649–2654.
- 49 F.-L. Mi, H.-W. Sung and S.-S. Shyu, *J. Appl. Polym. Sci.*, 2001, **81**, 1700–1711.
- 50 S. Karan, Z. Jiang and A. G. Livingston, *Science*, 2015, **348**, 1347–1351.
- 51 M. Nikbakht Fini, J. Zhu, B. Van der Bruggen, H. T. Madsen and J. Muff, *J. Membr. Sci.*, 2020, **612**, 118458.
- 52 C. Y. Tang, Y.-N. Kwon and J. O. Leckie, *J. Membr. Sci.*, 2007, **287**, 146–156.
- 53 S. R. Hosseinabadi, K. Wyns, V. Meynen, A. Buekenhoudt and B. Van der Bruggen, *J. Membr. Sci.*, 2016, **513**, 177–185.
- 54 Y. Li, S. Yuan, C. Zhou, Y. Zhao and B. Van der Bruggen, *J. Mater. Chem. A*, 2018, **6**, 22987–22997.
- 55 D. Lv, M. Zhu, Z. Jiang, S. Jiang, Q. Zhang, R. Xiong and C. Huang, *Macromol. Mater. Eng.*, 2018, **303**, 1800336.
- 56 S. Agarwal and A. Greiner, *Polym. Adv. Technol.*, 2011, **22**, 372–378.
- 57 H. Y. Nguyen Thi, S. Kim, B. T. Duy Nguyen, D. Lim, S. Kumar, H. Lee, G. Szekely and J. F. Kim, *ACS Sustainable Chem. Eng.*, 2022, **10**, 2532–2544.
- 58 R. Hardian, R. M. Cywar, E. Y. X. Chen and G. Szekely, *J. Membr. Sci. Lett.*, 2022, **2**, 100016.
- 59 W. Xie, G. M. Geise, B. D. Freeman, H.-S. Lee, G. Byun and J. E. McGrath, *J. Membr. Sci.*, 2012, **403–404**, 152–161.
- 60 M. Jahanshahi, A. Rahimpour and M. Peyravi, *Desalination*, 2010, **257**, 129–136.
- 61 L. Shao, X. Q. Cheng, Y. Liu, S. Quan, J. Ma, S. Z. Zhao and K. Y. Wang, *J. Membr. Sci.*, 2013, **430**, 96–105.
- 62 W.-Z. Qiu, G.-P. Wu and Z.-K. Xu, *ACS Appl. Mater. Interfaces*, 2018, **10**, 5902–5908.

